J. Fluid Mech. (2011), *vol.* 679, *pp.* 628–640.
doi:10.1017/jfm.2011.163

Hydroelastic solitary waves in deep water

PAUL A. MILEWSKI[1]†, J.-M. VANDEN-BROECK[2] AND ZHAN WANG[1]

[1]Department of Mathematics, University of Wisconsin-Madison, Madison, WI 53706, USA
[2]Department of Mathematics, University College London, London WC1E 6BT, UK

(Received 9 January 2011; revised 29 March 2011; accepted 31 March 2011; first published online 19 May 2011)

The problem of waves propagating on the surface of a two-dimensional ideal fluid of infinite depth bounded above by an elastic sheet is studied with asymptotic and numerical methods. We use a nonlinear elastic model that has been used to describe the dynamics of ice sheets. Particular attention is paid to forced and unforced dynamics of waves having near-minimum phase speed. For the unforced problem, we find that wavepacket solitary waves bifurcate from nonlinear periodic waves of minimum speed. When the problem is forced by a moving load, we find that, for small-amplitude forcing, steady responses are possible at all subcritical speeds, but for larger loads there is a transcritical range of forcing speeds for which there are no steady solutions. In unsteady computations, we find that if the problem is forced at a speed in this range, very large unsteady responses are obtained, and that when the forcing is released, a solitary wave is generated. These solitary waves appear stable, and can coexist within a sea of small-amplitude waves.

Key words: elastic waves, solitary waves, surface gravity waves

1. Introduction

We consider the problem of surface waves on a semi-infinite incompressible inviscid fluid in two-dimensions bounded above by a flexible elastic sheet. The two competing restoring forces are gravity and the flexural elasticity of the sheet, and hence we denote this problem as the fluid flexural-gravity (FG) wave problem. We shall use the irrotational Euler equations with the fully nonlinear kinematic and dynamic boundary conditions for the fluid, and, for the solid, use the simplest Kirchoff–Love nonlinear elasticity model appropriate for thin flexible sheets as in Parau & Dias (2002) and Bonnefoy, Meylan & Ferrant (2009). This elasticity model yields a restoring force in the form of a pressure jump across the elastic sheet equal to

$$D\partial_x^2\kappa, \tag{1.1}$$

where D is the flexural rigidity of the sheet and κ is its curvature. The principal approximation made here is that the sheet is thin, and that its inertia and its stretching (or the existence of a pre-stressed state) are neglected. At first sight, the formulation for this problem appears similar to that of the gravity–capillary wave problem where the pressure jump across the free surface is proportional to its curvature. Despite this similarity, the phenomena observed in the two problems are quite different and we shall highlight these differences below. More details on the bifurcations of

† Email address for correspondence: milewski@math.wisc.edu

the FG wave problem with a pre-stressed sheet modelled with the inclusion of a surface-tension-like term can be found in Il'ichev (2000).

Fluid FG models have been used to study waves generated by moving loads on a thin ice sheet floating over water. A thorough treatment of the linear problem under various modelling assumptions together with an extensive review of experimental work is found in Squire *et al.* (1996). A particularly interesting case is that of near-critical forcing which occurs when the load moves at a speed close to the minimum phase speed of linear waves. In that case, the free-surface displacement can be large and nonlinear effects may be important: at criticality, the linear elastic plate theory predicts a displacement that grows unbounded with time. Squire *et al.* (1988) and Takizawa (1988) measured the response of an ice sheet under moving loads with particular attention to this regime and it is the nonlinear resolution of this issue that inspired the work of Parau & Dias (2002) on the steady response. The nonlinear unsteady moving load problem, together with an alternative numerical formulation to that presented here (based on a truncation of the Dirichlet-to-Neumann map for the potential fluid flow), was considered by Bonnefoy *et al.* (2009). A further resolution of the unbounded displacement prediction that also addresses some observational features is the inclusion of damping through a viscoelastic plate model designed to better represent the material properties of ice, when the predicted response due to a steadily moving load remains pronounced but finite at criticality (Hosking, Sneyd & Waugh 1988; Wang, Hosking, & Milinazzo 2004).

In the present paper, we shall focus on both steady and dynamic phenomena of *free* solitary waves with length scales in the vicinity of the *minimum* of the dispersion relation which corresponds to the case where elastic and gravitational restoring forces are comparable. Both localized and generalized solitary waves are found to bifurcate from large-amplitude periodic waves. We also show that these waves may arise naturally from the moving load problem in a transcritical forcing regime which occurs *only* for sufficiently large loads. In order to give the reader an idea of the scales involved in ice sheets in the conditions of the aforementioned experimental measurements, D ranged from 10^5 to 10^9 N m, corresponding to a minimum-speed wavelength in the range 20–160 m and depending mainly on the thickness of the ice (which varied from 17 to 160 cm).

Analysis and numerical computations of free waves on the FG problem of the type we consider were pioneered, in the periodic case, by Forbes (1986). In Parau & Dias (2002), free solitary waves were briefly considered in the 'shallower' case (see below). More recently, further results on periodic waves, generalized solitary waves and three-dimensional waves were obtained by Vanden-Broeck & Parau (2011) and Parau & Vanden-Broeck (2011). A related problem with a longer history is that of unstable fluid–elastic interactions such as the recent work of Peake (2001) and references therein. In that regime, gravity is usually neglected, the inertia of the elastic sheet and its stretching are included, and the addition of a mean flow leads to instabilities. There have also been rigorous results on the FG wave problem: recently, Toland (2008) proved the existence of periodic waves and introduced an energetically consistent elastic model on which we shall comment later. A review of bifurcations leading to solitary waves in a variety of fluid problems, including in ice-sheet modelling problems, is found in Il'ichev (2000).

Much can be learned from the dispersion relation for the linearized FG model. Note that $(D/\rho g)^{1/4}$ and $(D/\rho g^5)^{1/8}$ are the characteristic length and time scales at which the restoring effects of flexural rigidity and gravity balance. Using these to non-dimensionalize the problem, the FG dispersion relation for an elastic sheet over

a fluid of dimensionless depth H is

$$c^2 = \tanh(kH)\left(\frac{1}{|k|} + |k|^3\right), \tag{1.2}$$

where c is the wave speed and k is the wavenumber. For all values of the depth H, $c = \sqrt{H}$ is a local maximum at $k = 0$ and there is a global minimum of phase speed c^* at k^*. For large k, $c \sim |k|^{3/2}$. These features imply that shallow-water-type generalized solitary waves may bifurcate from $k = 0$, which is the case considered in Vanden-Broeck & Parau (2011), and that wavepacket-type solitary waves may bifurcate from k^*. In this paper, we concentrate on the latter case. In Parau & Dias (2002), using a weakly nonlinear normal-form analysis of the free and forced problem around this minimum, they find that there is a critical depth H_c above which there are no free solitary waves bifurcating from a uniform stream. For depths shallower than H_c, their analysis shows that there are solitary waves and they compute these waves using a fully nonlinear boundary-integral method. They also consider the problem forced by a load moving at speed U. In this case and for the type of forcing they use, they find that for $H < H_c$ the branch of forced solutions exists only up to a speed $U^* < c^*$, whereas if $H > H_c$ this branch continues up to $c = c^*$. In contrast, we focus here on infinite depth (as a model for $H > H_c$) and extend their results in several ways as described below.

The existence of weakly nonlinear wavepacket solitary waves bifurcating from the minimum of a phase-speed dispersion curve can be deduced from the nonlinear Schödinger (NLS) equation governing the modulation of a carrier surface displacement wave with wavenumber near k^*:

$$\mathrm{i}A_T + \lambda A_{XX} = \mu|A|^2 A. \tag{1.3}$$

If the product of the coefficients $\lambda(H)\mu(H) < 0$, the equation is of the focusing type, and there exist sech-type solitary waves for the NLS equation. Since at a minimum of $c(k)$ the phase and group speed are equal, these NLS solitary waves approximate the envelope of the wavepacket solitary waves of the original system. In the FG problem, the sign of the dispersive coefficient λ is positive at k^* for all values of H (which follows directly from the fact that c is a minimum there), but the sign of the nonlinearity coefficient μ changes at H_c, with $\mu > 0$ for $H > H_c$. This fact disallows solitary waves from bifurcating about the uniform state in deeper water. We shall show in this paper that solitary waves *do* occur in deeper water, but they are a new type in that they occur along a branch of generalized solitary waves that itself bifurcates from periodic waves of *finite amplitude*. For simplicity, in this paper, we shall assume that the water is infinitely deep, although we are confident the results apply for all $H > H_c$. We also consider here the *forced* problem of the response to a travelling load. We find that, for sufficiently large loads, no steady solutions exist for a range of subcritical speeds and that in the time-dependent problem this gap yields very-large-amplitude unsteady behaviour, including the generation of solitary waves.

It is useful to compare the present problem with the problem of gravity–capillary (GC) waves (see, for example, Vanden-Broeck 2010). In the GC problem, when the Bond number B (the inverse of a dimensionless depth squared) is below $1/3$, corresponding to 'deep' water, the dispersion relation is qualitatively similar to the FG problem having a minimum at finite k. However, the corresponding NLS equation in that GC regime *always* supports wavepacket solitary waves since the coefficients are of the appropriate sign. One concludes from this that the 'shallow' regime ($H < H_c$)

of the FG problem is – from the perspective of bifurcation theory – qualitatively similar to the deep regime $B < 1/3$ of the GC problem. It is in this case that Parau & Dias (2002) compute some free solitary waves. The deep ($H > H_c$) regime of the FG problem has no equivalent in the GC problem. It should be noted that the shallow regime of GC waves ($B > 1/3$) also supports (generalized) solitary waves; however, these are not of the wavepacket-type since they bifurcate from $k = 0$.

This paper is structured as follows. In § 2, we briefly present a time-dependent conformal mapping technique for the full problem, its reduction for the travelling wave problem, and the linear and weakly nonlinear behaviour. In § 3, we present forced and unforced numerical travelling-wave results, focusing on solitary waves and present typical time-dependent forced behaviour. In the conclusions, we discuss possible mathematical modelling extensions to the work.

2. Formulation

Consider a two-dimensional, irrotational flow of an inviscid, incompressible fluid of infinite depth bounded above by an elastic sheet. Denoting the free surface by $y = \bar{\zeta}(x, t)$ and the velocity potential by $\bar{\phi}(x, y, t)$, the governing equations for the flow and the nonlinear boundary conditions are

$$\Delta\bar{\phi} = 0 \qquad \text{for } -\infty < y < \bar{\zeta}(x, t), \tag{2.1}$$

$$\bar{\phi} \to 0 \qquad \text{as } y \to -\infty, \tag{2.2}$$

$$\bar{\zeta}_t + \bar{\phi}_x\bar{\zeta}_x = \bar{\phi}_y \qquad \text{at } y = \bar{\zeta}(x, t), \tag{2.3}$$

$$\bar{\phi}_t = -\frac{1}{2}\left[\bar{\phi}_x^2 + \bar{\phi}_y^2\right] - \bar{\zeta} - \partial_{xx}\frac{\bar{\zeta}_{xx}}{\left(1 + \bar{\zeta}_x^2\right)^{3/2}} - \bar{P} \qquad \text{at } y = \bar{\zeta}(x, t). \tag{2.4}$$

The term $\bar{P}(x, t)$ is the dimensionless pressure distribution exerted by a load on the elastic sheet. These equations have been made dimensionless by choosing

$$\left(\frac{D}{\rho g}\right)^{1/4}, \quad \left(\frac{D}{\rho g^5}\right)^{1/8}, \quad \left(\frac{Dg^3}{\rho}\right)^{1/8}, \quad (D\rho^3 g^3)^{1/8}, \tag{2.5}$$

as the units of length, time, velocity and pressure, where ρ is the density of the fluid and g is the acceleration due to gravity.

In order to handle the unknown free-surface computationally, we reformulate this system using a time-dependent conformal map from the physical domain to the lower half-plane with horizontal and vertical coordinates denoted by ξ and η, respectively. Such a method was used by Dyachenko, Zakharov & Kuznetsov (1996), Li, Hyman & Choi (2004) and Milewski, Vanden-Broeck & Wang (2010). The map can be found by solving the harmonic boundary-value problem

$$y_{\xi\xi} + y_{\eta\eta} = 0 \qquad \text{for } -\infty < \eta < 0, \tag{2.6}$$

$$y = Y(\xi, t) \qquad \text{at } \eta = 0, \tag{2.7}$$

$$y \sim \eta \qquad \text{as } \eta \to -\infty, \tag{2.8}$$

where $Y(\xi, t) = \bar{\zeta}(x(\xi, 0, t), t)$. The harmonic conjugate variable $x(\xi, \eta, t)$ is defined through the Cauchy–Riemann relations for the complex function $z(\xi, \eta, t) = x(\xi, \eta, t) + \mathrm{i}y(\xi, \eta, t)$. In the transformed plane, the velocity potential $\phi(\xi, \eta, t) \triangleq \bar{\phi}(x(\xi, \eta, t), y(\xi, \eta, t), t)$ and its harmonic conjugate $\psi(\xi, \eta, t)$ also satisfy Laplace's

equation. Thus,

$$\begin{aligned} \phi_{\xi\xi} + \phi_{\eta\eta} &= 0 \quad && \text{for } -\infty < \eta < 0, \\ \phi &= \Phi(\xi, t) && \text{at } \eta = 0, \\ \phi &\to 0 && \text{as } \eta \to -\infty, \end{aligned}$$

where $\Phi(\xi, t) \triangleq \phi(\xi, 0, t)$. Defining $\Psi(\xi, t) \triangleq \psi(\xi, 0, t)$ and $X(\xi, t) \triangleq x(\xi, 0, t)$, from elementary harmonic analysis, we have

$$\Psi = \mathscr{H}[\Phi], \quad X = \xi - \mathscr{H}[Y], \tag{2.9}$$

where $\mathscr{H}$ is the Hilbert transform,

$$\mathscr{H}[f] = \int_{-\infty}^{\infty} \frac{f(\xi', 0, t)}{\xi' - \xi} \, \mathrm{d}\xi'. \tag{2.10}$$

Next, we shall write the evolution equations for Y and Φ using the boundary conditions at the free surface. The details (with the exception of the tedious computation of the restoring force of the sheet) can be found in Milewski *et al.* (2010) and follow from the application of the chain rule on $Y(\xi, t) = \bar{\zeta}(x(\xi, 0, t), t)$, $\Phi(\xi, t) = \bar{\phi}(x(\xi, 0, t), y(\xi, 0, t), t)$ and $\Psi(\xi, t) = \bar{\psi}(x(\xi, 0, t), y(\xi, 0, t), t)$. The result is the surface Euler system

$$X_\xi = 1 - \mathscr{H}[Y_\xi], \tag{2.11}$$

$$\Psi_\xi = \mathscr{H}[\Phi_\xi], \tag{2.12}$$

$$Y_t = Y_\xi \mathscr{H}\left[\frac{\Psi_\xi}{J}\right] - X_\xi \left(\frac{\Psi_\xi}{J}\right), \tag{2.13}$$

$$\Phi_t = \frac{1}{2}\frac{\Psi_\xi^2 - \Phi_\xi^2}{J} - Y - \frac{M}{X_\xi^3 J^{7/2}} + \Phi_\xi \mathscr{H}\left[\frac{\Psi_\xi}{J}\right] - P, \tag{2.14}$$

where $J = X_\xi^2 + Y_\xi^2$, $P(\xi, t) = \bar{P}(x(\xi, 0, t), t)$, and the bending term M is given by

$$\begin{aligned} M = &-X_\xi X_{\xi\xi\xi\xi} Y_\xi^5 - 2X_\xi^3 X_{\xi\xi\xi\xi} Y_\xi^3 - X_\xi^5 X_{\xi\xi\xi\xi} Y_\xi - 4X_\xi^5 X_{\xi\xi\xi} Y_{\xi\xi} - 6X_\xi^5 X_{\xi\xi} Y_{\xi\xi\xi} \\ &+ X_\xi^2 Y_\xi^4 Y_{\xi\xi\xi\xi} + 2X_\xi^4 Y_\xi^2 Y_{\xi\xi\xi\xi} - 15X_\xi^3 X_{\xi\xi}^3 Y_\xi + 12X_\xi^2 Y_\xi^2 Y_{\xi\xi}^3 + 15X_\xi^4 X_{\xi\xi}^2 Y_{\xi\xi} \\ &- 3X_\xi^3 X_{\xi\xi} Y_\xi^2 Y_{\xi\xi\xi} + 3X_\xi X_{\xi\xi} Y_\xi^4 Y_{\xi\xi\xi} + X_\xi^3 X_{\xi\xi\xi} Y_\xi^2 Y_{\xi\xi} + 5X_\xi X_{\xi\xi\xi} Y_\xi^4 Y_{\xi\xi} \\ &- 33X_\xi^2 X_{\xi\xi}^2 Y_\xi^2 Y_{\xi\xi} - 3X_{\xi\xi}^2 Y_\xi^4 Y_{\xi\xi} + 10X_\xi^4 X_{\xi\xi} X_{\xi\xi\xi} Y_\xi + 11X_\xi^2 X_{\xi\xi} X_{\xi\xi\xi} Y_\xi^3 \\ &+ X_{\xi\xi} X_{\xi\xi\xi} Y_\xi^5 - 9X_\xi^2 Y_\xi^3 Y_{\xi\xi} Y_{\xi\xi\xi} - 9X_\xi X_{\xi\xi} Y_\xi^3 Y_{\xi\xi}^2 - 9X_\xi^4 Y_\xi Y_{\xi\xi} Y_{\xi\xi\xi} \\ &- 3X_\xi^4 Y_{\xi\xi}^3 + 36X_\xi^3 X_{\xi\xi} Y_\xi Y_{\xi\xi}^2 + X_\xi^6 Y_{\xi\xi\xi\xi}. \end{aligned} \tag{2.15}$$

Given initial values for Φ and Y, X_ξ and Ψ_ξ can be calculated with the first two equations of (2.11)–(2.14), and Φ and Y can then be advanced in time with the last two equations.

2.1. *Travelling waves*

Seeking travelling-wave solutions to the Euler equations (2.1)–(2.4) with wave speed c, we assume that all functions depend on $x - ct$ and replace (2.3) and (2.4) with

$$-c\bar{\zeta}_x = -\bar{\phi}_x \bar{\zeta}_x + \bar{\phi}_y, \tag{2.16}$$

$$-c\bar{\phi}_x = -\frac{1}{2}\left[\bar{\phi}_x^2 + \bar{\phi}_y^2\right] - \bar{\zeta} - \partial_{xx} \frac{\bar{\zeta}_{xx}}{(1 + \bar{\zeta}_x^2)^{3/2}} - P. \tag{2.17}$$

Following the same conformal mapping as in the previous section, the kinematic boundary condition becomes $\Psi = cY$, then the dynamic boundary condition becomes

$$\frac{c^2}{2}\left(\frac{1}{J}-1\right)+Y+\frac{M}{X_\xi^3 J^{7/2}}+P=0. \tag{2.18}$$

Equation (2.18), together with $X_\xi = 1-\mathscr{H}[Y_\xi]$, completes an integro-differential system for Y. From the solution Y, Φ can be found using $\Phi = -c\mathscr{H}[Y]$. The present formulation for travelling waves is equivalent to that of Parau & Dias (2002) under a different scaling.

2.2. *Linear and weakly nonlinear waves*

The dispersion relation of the system can be obtained directly from (2.1)–(2.4) or can be recovered by linearizing the surface Euler system by taking Y, Φ_ξ, Ψ_ξ small and $X_\xi \sim 1$, $J \sim 1$. This results in the dispersion relation

$$\omega^2 = |k|(1+k^4) \quad \text{or} \quad c^2 = \left(\frac{1}{|k|}+|k|^3\right). \tag{2.19}$$

We consider solitary waves bifurcating from the phase-speed minimum

$$k^* = \left(\frac{1}{3}\right)^{1/4} \approx 0.7598, \quad c^* = \sqrt{3^{1/4}+3^{-3/4}} \approx 1.3247. \tag{2.20}$$

In order to derive the NLS equation governing modulations of a monochromatic wave, one substitutes the ansatz

$$\begin{pmatrix}\bar{\xi}\\ \bar{\phi}\end{pmatrix} \sim \epsilon \begin{pmatrix}A(X,T)\\ B(X,T)\,\mathrm{e}^{|k|y}\end{pmatrix}\mathrm{e}^{\mathrm{i}(kx-\omega t)} + \text{c.c.} + \epsilon^2\begin{pmatrix}\zeta_1\\ \phi_1\end{pmatrix} + \epsilon^3\begin{pmatrix}\zeta_2\\ \phi_2\end{pmatrix} + \cdots, \tag{2.21}$$

where $T = \epsilon^2 t$, $X = \epsilon(x - c_g t)$, c.c. indicates the complex conjugate of the preceding term and c_g is the group velocity, into (2.1)–(2.4), and ensures that the series is well-ordered for $t = O(\epsilon^{-2})$. We omit the details of the derivation and state the result for the carrier wave k^*. The envelopes A satisfy the NLS equation (with B slaved to A):

$$\mathrm{i}A_T + \lambda A_{XX} = \mu|A|^2 A, \quad B = -\mathrm{i}c^* A, \tag{2.22}$$

with coefficients

$$\lambda = \frac{3^{7/8}}{2}, \quad \mu = \frac{79}{88}3^{-9/8}. \tag{2.23}$$

Since $\lambda\mu > 0$, the NLS equation is of the defocusing type and one does not expect small-amplitude solitary waves to exist for $c < c^*$. The NLS analysis, however, predicts a branch of periodic waves with $c > c^*$ bifurcating from a uniform flow. These periodic solutions are Stokes' waves and have the speed-amplitude dependence

$$c - c^* = \frac{\mu}{4k^*}|\zeta_{max}|^2, \tag{2.24}$$

which can be obtained from NLS solutions of the form $A = a\,\mathrm{e}^{-\mathrm{i}\Omega \mathrm{T}}$, with $\Omega = \mu a^2$.

2.3. *Computational methods*

The numerical integration of the surface Euler system is accomplished with a Fourier spectral discretization of the ξ dependence, where all derivatives and Hilbert transforms are computed in Fourier space. For travelling waves, the system is solved using Newton's method where the unknowns are the Fourier coefficients and branches

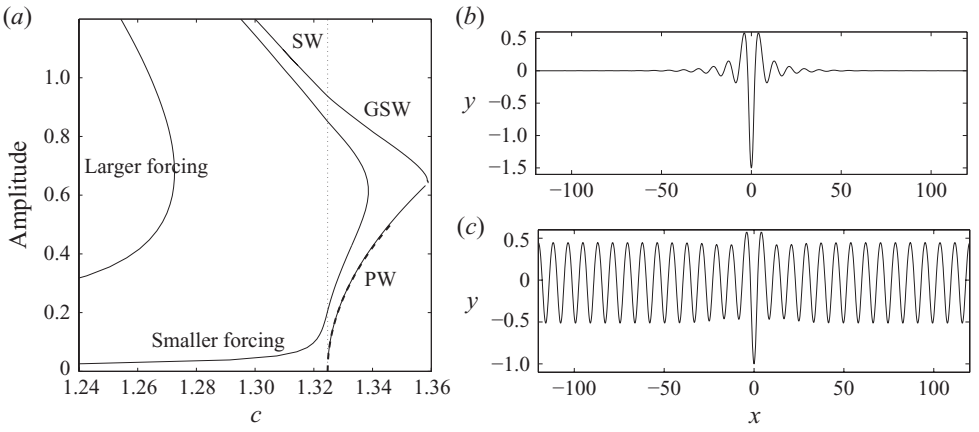

FIGURE 1. (*a*) Travelling wave solution branches near the minimum speed c^* (which is shown by the vertical line). Branches of forced solutions are shown by two different forcing amplitudes, $a = 0.2$ and $a = 0.02$. The uppermost curve is a branch of unforced solitary waves for $c < c^*$ (labelled SW) and generalized solitary waves for $c > c^*$ (labelled GSW). The branches originating at c^* are periodic Stokes solutions (labelled PW) and they are compared to the NLS prediction (thick dashed curve). The amplitude parameter is $\frac{1}{2}[\max(Y) - \min(Y)]$. Examples of (*b*) unforced solitary waves and (*c*) generalized solitary waves.

are computed through straightforward continuation methods. For time-dependent solutions, a fourth-order Runge–Kutta method is used and products are computed in real space and dealiazed with a doubling of Fourier modes. Typically, for bifurcation diagrams of travelling waves, 64–2048 Fourier modes provide accurate solutions. In order to compute time-dependent solutions on large enough domains, 2048 modes were used. The method was shown to be highly accurate in CG waves (Milewski *et al.* 2010). Although some waves 'wrap around' in our computations, they do not affect the qualitative dynamics. In computing the forced travelling-wave problem, we used the pressure distribution $\bar{P} = a\,\mathrm{e}^{(x-st)^2/16}$, and results are qualitatively similar for other distributions.

3. Results

In the forced travelling-wave problem we note that there are two localized steady solutions for certain subcritical speeds: one of smaller amplitude and the other of larger amplitude (see figure 1). The solutions of smaller amplitude are a perturbation of the free stream, and those of larger amplitudes are perturbed free solitary waves. Note, however, that at larger *forcing* amplitudes, there are no steady solutions for a range of transcritical forcing speeds, $c_{max} < s < c^*$. Here, c_{max} is defined as the largest speed at which there is a steady solution for a fixed forcing amplitude (i.e. where the branch of forced solutions turns around). This range or 'gap' will lead to interesting time-dependent dynamics.

The branch of free solitary waves can be obtained by reducing the forcing to zero from the large-amplitude forced solutions. Once the solitary wave branch is found, as one reduces the amplitude along the branch, the solitary waves become generalized–solitary waves when $c > c^*$. This happens due to a resonance with periodic waves of speed c. As the amplitude of the central trough is further reduced, the 'tails' of the generalized solitary wave increase in amplitude until the branch terminates on a branch of finite-amplitude Stokes' waves.

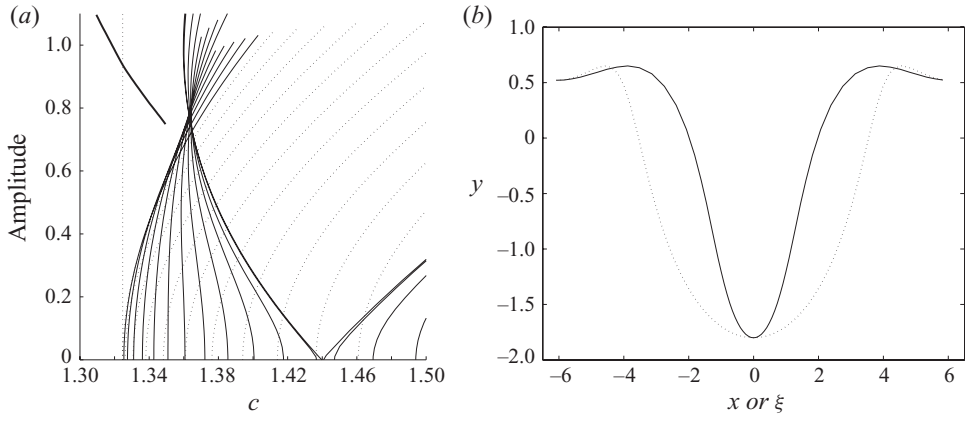

FIGURE 2. (*a*) Families of finite-amplitude Stokes periodic waves with $c > c^*$ (c^* is indicated by the vertical line), bifurcating from zero amplitude for various $k < k^*$ (solid curves) and $k > k^*$ (dotted curves). The thick curve is a portion of the branch of solitary and generalized–solitary waves shown in figure 1. The amplitude parameter is $\frac{1}{2}[\max(Y) - \min(Y)]$. (*b*) Large-amplitude 'Wilton' waves shown both as a function of ξ (dotted line) and x (solid line).

In addition to these branches, we also show in figure 1 the branch of Stokes periodic waves bifurcating from the minimum of the dispersion relation, the corresponding prediction from the NLS equation, and sample profiles of the solitary and generalized solitary waves. In the nomenclature used in GC waves, the solitary waves we computed are called depression solitary waves. We attempted to compute elevation solitary waves, whose free-surface displacement is positive at the centre and which exist in the GC problem, but were unsuccessful. Solitary waves of small amplitude of were not found, as expected from the NLS analysis.

In order to better understand the origin of the large-amplitude generalized solitary waves, we compute a more complete bifurcation diagram of periodic waves, as shown in figure 2. For various values of k near k^*, branches of Stokes waves with period $2\pi/k$ are shown. For small amplitudes, it is the wave with $2\pi/k^*$ periodicity that has the lowest speed; however, at fixed higher amplitudes this is no longer the case. Progressively longer waves with $k < k^*$ have the minimum speed, up to a fold point where the minimum speed wave occurs on the branch corresponding, at small amplitude, to 'Wilton' ripples. For more details on Wilton ripples in this context, see Vanden-Broeck & Parau (2011). This branch is the left solid curve originating at $c \approx 1.44$ in figure 2. The solitary and generalized solitary wave branch is also shown in this figure, and it appears that generalized solitary waves occur only when there are no periodic waves of the same speed and larger amplitudes. The computation of the generalized solitary wave branch near its bifurcation point is very sensitive to the size of the computational domain, which selects a particular periodicity, and we only show the curve where we are confident that it does not depend on the domain size. Incidentally, the diverging branches of Wilton-like ripples in figure 2 clearly explain the phenomenon observed by Bonnefoy *et al.* (2009), where the periodic wavetrain generated by a moving load changes abruptly in behaviour when the load speed is varied in the vicinity of $c \approx 1.44$.

We now turn to time-dependent solutions, particularly to the case of subcritical localized forcing. Physically, we investigate the response of a moving load on ice-covered deep water at near-critical speeds (Parau & Dias 2002). In many situations,

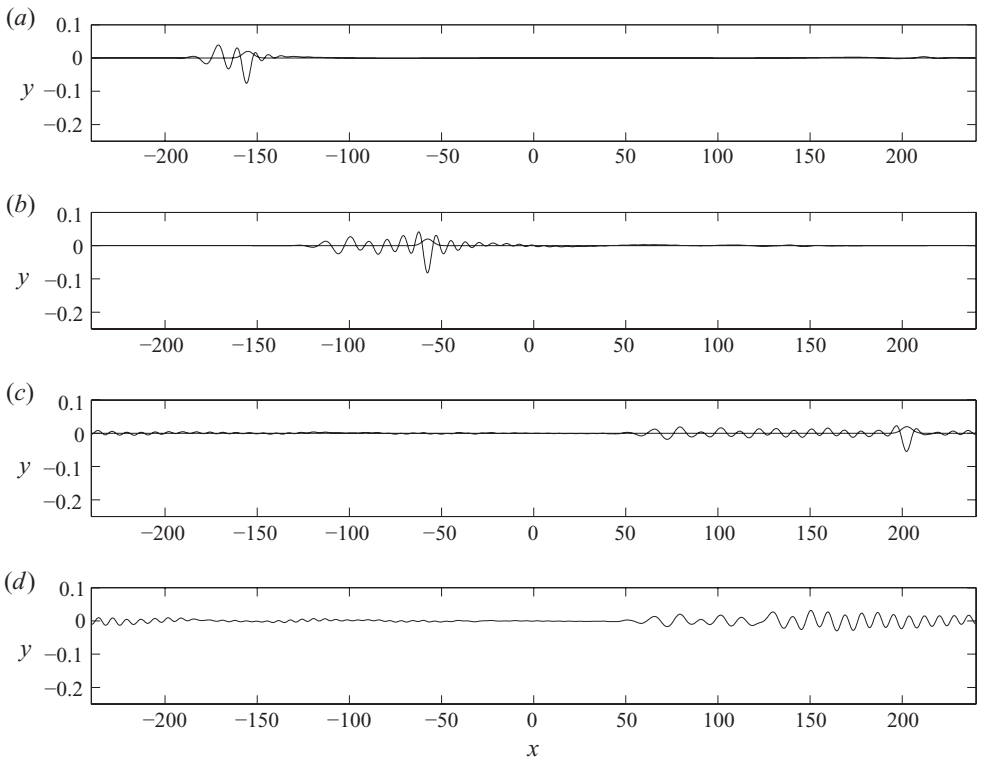

FIGURE 3. Time-dependent computation of the free surface due to a subcritically moving force at smaller forcing amplitudes ($a = 0.02$, $s = 1.3$). The forcing is kept on throughout the computation. (*a–c*) $t = 50$, 125, 325. (*d*) The solution at $t = 325$, in a case where the forcing is turned off at $t = 125$. The forcing is also shown.

the response to a moving force in free-surface fluid problems is strongest and fundamentally nonlinear when the speed s of the forcing is slightly below a minimum or above a maximum of the phase speed of free dispersive waves, since there is a near resonance and there is no linear mechanism to radiate the energy. For each localized forcing in this case, there exists a range of forcing speeds (the transcritical regime) for which there is no travelling solution to the problem. Within this range the forcing is called *resonant* and one observes complex time-dependent solutions often involving the periodic shedding of solitary waves. Examples are Wu (1987) for surface water waves in shallow water, Grimshaw & Smith (1986) for internal waves and Berger & Milewski (2000) for shallow three-dimensional GC flows. In these examples, however, the transcritical regime exists for arbitrarily small forcing amplitudes. This fact is a consequence of these problems having solitary waves that exist down to zero amplitude. Since the branches of forced solutions are a perturbation of the free solitary wave branch, arbitrarily small forcing will break the symmetry of the bifurcation and create a gap in the existence of steady solutions. In the present situation, this is not the case: the transcritical regime exists only for sufficiently large forcing (see figure 1).

Two representative cases of time-dependent evolution are shown, both using $s = 1.3$. A small forcing case ($a = 0.02$) in which there is no transcritical regime is shown in figure 3, and a larger forcing case ($a = 0.2$), in which the forcing speed is in the transcritical range, in figure 4. The behaviour of both cases is qualitatively very

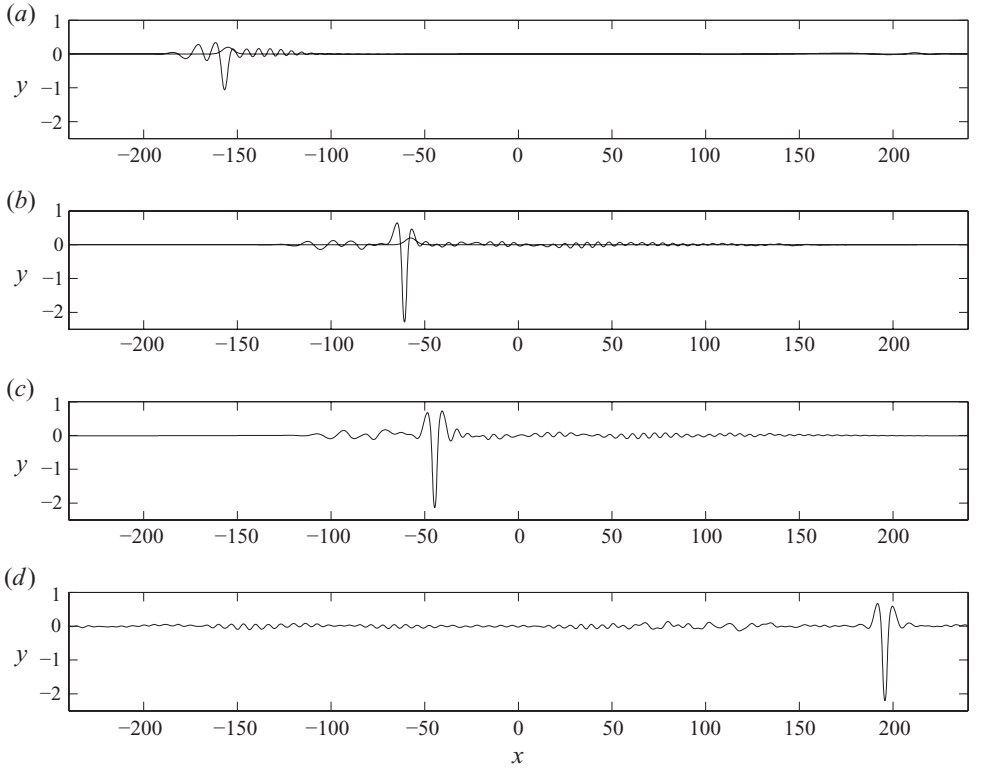

FIGURE 4. Time-dependent computation of the free surface due to a subcritically moving force at larger forcing amplitudes ($a = 0.2$, $s = 1.3$). The forcing was switched on at $t = 0$, $x = -220$ and switched off at $t = 125$. The solution, together with the forcing, is shown in (a–d) at times $t = 50$, 125, 137.5, 325, respectively. The forcing is also shown.

different. For the smaller forcing, as shown in figure 1, there is a small-amplitude steady response to the forcing. In the time-dependent dynamics (see figure 3a–c), the amplitude of the response remains small and close to the steady solution in the vicinity of the forcing. There are, however, unsteady upstream and downstream waves present due to the impulsive start of the forcing. For a larger forcing, if the speed of the forcing lies in the gap for which steady solutions do not exist (see figure 1), the response is much stronger. In this case, the time-dependent solutions grow in amplitude and become steeper up to a point at which our numerical method fails (we have computed solutions where the slope is greater than 2.5). We do not observe a periodic shedding of solitary waves as observed in other transcritical forcing regimes.

In the computation of figure 4 the forcing was turned off after a period of time ($t = 125$). Snapshots in figure 4(b,c) are immediately before and shortly after the forcing is switched off. We note that the solution rapidly relaxes to a symmetric solitary wave. The last snapshot (figure 4d) shows that the solitary wave persists for long times in the midst of smaller linear waves. From longer computations (not shown), we believe that these solitary waves are stable and robust. For the smaller forcing of figure 3, we do not have any problems continuing the forced computation for arbitrary long times, but, for comparison, we show the final profile of a numerical experiment in which the smaller load has also been removed at $t = 125$ (see figure 3d).

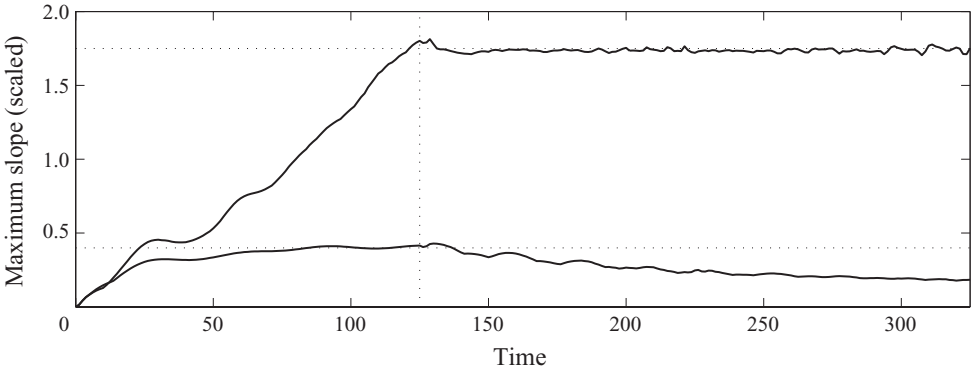

FIGURE 5. Maximum slope of the free surface as a function of time for the computations shown in figures 3 and 4. The forcing was turned off at $t = 125$. The lower curve has been vertically magnified by a factor of 10 to reflect the difference in forcing amplitude.

In this case, the disturbances disperse away and do not form the solitary wave seen in figure 4. The contrast between the two regimes can be clearly seen in figure 5: here we show the maximum slope of the elastic sheet as a function of time for the computations described above. For the large forcing the approximate constancy of the maximum slope after $t = 125$ is a result of the generated solitary wave, whereas in the small forcing, the maximum slope decreases after the forcing is turned off as a result of dispersion. Note the *much* larger amplification factor for the transcritical regime (the small forcing curve has been scaled so the comparison is meaningful).

4. Conclusions

The bifurcation problem of deep water FG waves near the minimum of the dispersion relation is rich with Stokes, solitary and generalized solitary waves. In particular, solitary waves exist only at finite amplitude, which is, to our knowledge, novel in free-surface fluid problems. Furthermore, the near-critically forced problem has qualitatively different behaviour for small- and large-amplitude loads. This qualitative difference should be observable in experimental measurements.

A particularly interesting case that emerges and warrants further study is that of $H \approx H_c$ (recall that H_c is the transition at which the NLS equation predicts that small-amplitude solitary waves cease to exist). In this case, the coefficient of the cubic nonlinear term in the NLS equation is small and, under appropriate rescaling, we believe that the modulations of wavepackets would be well described by the cubic–quintic NLS equation (or, due to the influence of a mean-flow, a cubic–quintic Benney–Roskes–Davey–Stewartson-type model):

$$\mathrm{i}A_t + \lambda A_{XX} = \mu|A|^2A + \mathrm{i}\delta_1|A|^2A_X + \mathrm{i}\delta_2A^2\bar{A}_X + \gamma|A|^4A. \tag{4.1}$$

In this case, the coefficient μ is negative (focusing) for $H < H_c$ and positive (defocusing) otherwise, whereas we conjecture that γ is negative (focusing). There are interesting features of such a model. First, the equation has a rich set of solutions corresponding to periodic, solitary and generalized solitary travelling waves of the original system for $\mu > 0$ (Gagnon 1989). These provide an analytical picture of the finite amplitude bifurcation from Stokes to solitary waves. Second, given the quintic focusing term, time-dependent solutions to the NLS equation will have finite time singularities. This corresponds to a nonlinear focusing of wave energy, and whilst

these blow-up solutions are surely in a regime which does not reflect the original problem, they indicate the onset of a wave-collapse instability as has been observed in the three-dimensional gravity–capillary problem (Akers & Milewski 2009).

We also comment on other possible elastic models. In this paper, we chose a model which has been widely used and for which we can compare our results with those of others, but which does not have a clear conservation form for the elastic potential energy. Two other models that do have such an energy conservation principle are the linear elasticity case (denoted below by the subscript L) and a simple conservative nonlinear model appearing in Toland (2008) (denoted below by the subscript C). In these cases, the pressure jump is given, respectively, by

$$D\partial_x^4\eta \quad \text{and} \quad D\left(\partial_\alpha^2\kappa + \tfrac{1}{2}\kappa^3\right), \tag{4.2}$$

where α is arclength. The dimensionless elastic potential energy in these cases is given by

$$P_L = \int \frac{1}{2}\bar{\zeta}_{xx}^2\,\mathrm{d}x \quad \text{and} \quad P_C = \int \frac{1}{2}\kappa^2\,\mathrm{d}\alpha. \tag{4.3}$$

Then, the total energy of the system is given by

$$\frac{1}{2}\int \mathrm{d}x \int_{-\infty}^{\bar{\zeta}} \left(\bar{\phi}_x^2 + \bar{\phi}_y^2\right)\mathrm{d}y + \frac{1}{2}\int \bar{\zeta}^2\,\mathrm{d}x + P_{L,C}. \tag{4.4}$$

In the infinite depth case, these models should have qualitatively similar small amplitude behaviour. Their linear theories are identical to that of the present case (hence λ in the NLS equation is the same) and the respective nonlinear NLS coefficients are also positive:

$$\mu_L = \frac{14}{11}3^{-9/8} \quad \text{and} \quad \mu_C = \frac{1}{44}3^{-9/8}. \tag{4.5}$$

These merit further investigation, particularly the conservative case which, given the smallness of the NLS cubic coefficient, may be well described by a cubic–quintic NLS model even in infinite depth.

This work was supported by the EPSRC under grant GR/S47786/01 and by the Division of Mathematical Sciences of the National Science Foundation under grant NSF-DMS-0908077.

REFERENCES

Akers, B. & Milewski, P. A. 2009 A model equation for wavepacket solitary waves arising from capillary–gravity flows. *Stud. Appl. Math.* **122**, 249–274.

Berger, K. & Milewski, P. A. 2000 The generation and evolution of lump solitary waves in surface-tension-dominated flows. *SIAM J. Appl. Math.* **61**, 731–750.

Bonnefoy, F., Meylan, M. H. & Ferrant, P. 2009 Nonlinear higher-order spectral solution for a two-dimensional moving load on ice. *J. Fluid Mech.* **621**, 215–242.

Dyachenko, A. L., Zakharov, V. E. & Kuznetsov, E. A. 1996 Nonlinear dynamics on the free surface of an ideal fluid. *Plasma Phys. Rep.* **22**, 916–928.

Forbes, L. K. 1986 Surface waves of large amplitude beneath an elastic sheet. Part 1. High-order series solution. *J. Fluid Mech.* **169**, 409–428.

Gagnon, L. 1989 Exact traveling-wave solutions for optical models based on the nonlinear cubic–quintic Schrödinger equation. *J. Opt. Soc. Am.* A **6**, 1477–1483.

Grimshaw, R. H. J. & Smith, N. 1986 Resonant flow of a stratified fluid over topography. *J. Fluid Mech.* **169**, 429–464.

Hosking, R. J., Sneyd, A. D. & Waugh, D. W. 1988 Viscoelastic response of a floating ice plate to a steadily moving load. *J. Fluid Mech.* **196**, 409–430.

Il'ichev, A. 2000 Solitary waves in media with dispersion and dissipation (a review). *Fluid Dyn.* **35**, 157–176.

Li, Y. A., Hyman, R. J. M. & Choi, W. 2004 A numerical study of the exact evolution equations for surface waves in water of finite depth. *Stud. Appl. Math.* **113**, 303–324.

Milewski, P. A., Vanden-Broeck, J.-M. & Wang, Z. 2010 Dynamics of steep two-dimensional gravity–capillary solitary waves *J. Fluid Mech.* **664**, 466–477.

Parau, E. & Dias, F. 2002 Nonlinear effects in the response of a floating ice plate to a moving load. *J. Fluid Mech.* **460**, 281–305.

Parau, E. & Vanden-Broeck, J.-M. 2011 Three-dimensional waves under an ice sheet. *Trans. Phil. Soc.* (in press) doi:10.1098/rsta.2011.0115.

Peake, N. 2001 Nonlinear stability of a fluid-loaded elastic plate with mean flow. *J. Fluid Mech.* **434**, 101–118.

Squire, V. A., Hosking, R. J., Kerr, A. D. & Langhorne, P. J. 1996 *Moving Loads on Ice Plates* (Solid Mechanics and Its Applications). Kluwer.

Squire, V. A., Robinson, W. H., Langhorne, P. J. & Haskell, T. G. 1988 Vehicles and aircraft on floating ice. *Nature* **333**, 159–161.

Takizawa, T. 1988 Response of a floating sea ice sheet to a steadily moving load. *J. Geophys. Res.* **93**, 5100–5112.

Toland, J. F. 2008 Steady periodic hydroelastic waves. *Arch. Rat. Mech. Anal.* **189**, 325–362.

Vanden-Broeck, J.-M. 2010 *Gravity–Capillary Free-Surface Flows.* Cambridge University Press.

Vanden-Broeck, J.-M. & Parau, E. 2011 Two-dimensional generalised solitary waves and periodic waves under an ice sheet. *Trans. Phil. Soc.* (in press), doi:10.1098/rsta.2011.0108.

Wang, K., Hosking, R. J. & Milinazzo, F. 2004 Time-dependent response of a floating viscoelastic plate to an impulsively started moving load. *J. Fluid Mech.* **521**, 295–317.

Wu, T. Y. 1987 Generation of upstream advancing solitons by moving disturbances. *J. Fluid. Mech.* **184**, 75–99.